Degron tagging to label membrane-wrapped objects and probe membrane topology

Katharina B Beer^, Gholamreza Fazeli^, Linda Irmisch, Ann M Wehman*

Rudolf Virchow Center, University of Würzburg, Würzburg, Germany

^authors contributed equally
*corresponding author

Ann Wehman
Josef-Schneider-Str. 2 / D15
97080 Würzburg, Germany
Tel +49 931 31-81906
Fax +49 931 31-83255
ann.wehman@uni-wuerzburg.de

Abstract

Visualization of specific organelles in cells over background fluorescence can be challenging, especially when reporters localize to multiple places. Instead of trying to identify proteins enriched in specific membrane-wrapped objects, we used a selective degradation approach to remove reporters from the cytoplasm. Using the ZF1 degron in *C. elegans* embryos, we demonstrate specific labelling of organelles, including extracellular vesicles, as well as individual neighbouring membranes. We show that degron tagging facilitates long-term tracking of released cell debris and cell corpses, even during their uptake and phagolysosomal degradation. We also demonstrate how degron tagging can probe the topology of the nuclear envelope and plasma membrane during cell division, giving insight into protein and organelle dynamics. As degron tags are used in bacteria, yeast, plants, and animals, this approach will enable the specific labelling and tracking of proteins, vesicles, organelles, cell fragments, and cells in many model systems.

Introduction

Membranes form barriers that separate the cell from its environment and separate diverse subcellular compartments so that they can carry out distinct functions within cells[1]. As membrane bilayers are less than 10 nm in diameter, light microscopy techniques often struggle to distinguish neighbouring membranes[2]. Membranes are also highly dynamic, undergoing fusion and fission events during diverse budding processes, including endocytosis, vesicular trafficking, and ectocytosis[3]. Using light microscopy, it is difficult to tell when membranes have completed budding and have a closed topology. Therefore, techniques that allow specific labelling are required to visualize membrane dynamics and probe membrane topology in living cells.

Fluorescent imaging techniques are only as specific as the reporters used to visualize objects. Reporters binding specific phosphatidylinositol species are popular for studying membrane dynamics[4], but these lipids are often present on multiple objects, making it hard to distinguish or track individual objects. One example is during phagocytosis, when cellular debris or cell corpses are engulfed by the plasma membrane[5]. Both the corpse and engulfing cell plasma membranes contain the same phosphatidylinositol species, making it challenging to distinguish these membranes in living cells. Electron microscopy and super-resolution light microscopy can visualize the few tens of nm that separate the phagosome membrane from the corpse membrane, but these techniques rely on fixation, which makes it challenging to study dynamics[6]. Another example is extracellular vesicles released from cells. Vesicles that bud from the plasma membrane by ectocytosis contain the same protein and lipid species as the membrane they originate from[7], which makes it hard to distinguish released vesicles from the plasma membrane of neighbouring cells, as well as to follow the release and uptake of these vesicles *in vivo*. Thus, new approaches are needed to specifically label these objects.

To overcome these challenges, we repurposed selective degradation to visualize specific membrane objects. Degron-mediated degradation decreases target protein levels and is an alternative to RNA interference or genetic knockouts[8]. Degron motifs recruit ubiquitin ligases to polyubiquitinate target proteins, resulting in the proteasomal degradation of cytosolic proteins or the lysosomal degradation of transmembrane proteins[9]. Rather than using degron tagging as a loss-of-function technique, we used the degradation of degron-tagged reporters in the cytosol to specifically label certain cells, cell fragments, organelles, and vesicles.

Here, we used the zinc finger 1 (ZF1) degron from the *C. elegans* PIE-1 protein to drive the degradation of fluorescent reporters in developing *C. elegans* embryos. The ZF1 degron is a small 36 amino acid motif recognized by the SOCS-box protein ZIF-1, which binds to the elongin C subunit of a ubiquitin ligase complex[10]. ZIF-1 is expressed in sequential sets of differentiating somatic cells[11], resulting in a stereotyped pattern of degradation[10]. Fusing ZF1 to a target protein results in rapid degradation within 30 to 45 min of ZIF-1 expression[12]. Here,

we show that ZF1-tagged reporters protected by membranes are no longer accessible to ubiquitination and degradation. This results in background-free labelling of specific cells, organelles, and vesicles. This improvement in the signal-to-noise ratio enabled the visualization of extracellular vesicles *in vivo*, the long-term tracking of individual phagosomes, as well as distinguishing a corpse plasma membrane from the phagosome membrane *in vivo*. In addition, ZF1-tagging allowed us to measure the timing of nuclear envelope breakdown and abscission during cell division. The use of degron-tagged reporters thus provides a convenient method for investigating *in vivo* dynamics from the level of proteins to cells.

Results

To determine whether degron-tagged reporters would be useful for cell biological approaches, we first tested whether an endogenous degradation system was capable of degrading abundant reporter proteins and examined whether the increased proteasomal load had negative effects on cells. To show that degron tags can rapidly degrade membrane reporters, we tagged the PH domain of rat PLC1∂1 with the ZF1 degron from *C. elegans* PIE-1 and expressed it in worm embryos. Similar to an mCherry-tagged PH reporter (Fig. 1A), the cytosolic mCh::PH::ZF1 reporter initially localized to the plasma membrane (Fig. 1D). Thus, the degron tag did not disrupt the normal localization of the reporter.

ZF1-mediated degradation begins in somatic cells during the 4-cell stage, due to the onset of expression of the ubiquitin ligase adapter protein ZIF-1[11]. While the fluorescence of mCh::PH persists in developing embryos (Fig. 1B-C), mCh::PH::ZF1 is progressively degraded, starting with the anterior and dorsal cells (Fig. 1E-G, video 1). ZIF-1 is not expressed in the germ lineage, resulting in persistent fluorescence in a couple of posterior cells (Fig. 1E-F). ZIF-1 expression also does not occur in two small cell corpses at the anterior side of the embryo that are born during meiosis[11,13]. These polar bodies maintain mCh::PH::ZF1 fluorescence (arrowheads in Fig. 1). Thus, degron tagging was able to rapidly degrade a bright, exogenous reporter in cells where the reporter could be ubiquitinated.

As ZIF-1 has a number of known targets, whose proteasomal degradation is important for embryonic development[10], we tested whether the expression of ZF1-tagged reporters disrupted embryonic development. Stable transgenic strains expressing various ZF1-tagged reporters were fertile and had viable progeny that did not show a delay in cell cycle timing (Fig. S1). This suggests that degron reporters are well tolerated and do not disrupt embryonic development.

Degron reporters detect released extracellular vesicles

In addition to labelling the plasma membrane, mCh::PH and mCh::PH::ZF1 labelled endocytic vesicles within cells (arrows in Fig. 1). Some of these vesicles maintained their

fluorescence in the mCh::PH::ZF1 strain (video 1). As mCh::PH::ZF1 localized on the cytosolic face of vesicles would be accessible for ubiquitination and proteasomal degradation, the persistence of the degron reporter suggests that it is protected from proteasomal degradation by intervening membranes. We hypothesized that the PH::ZF1 reporter persists in extracellular vesicles or other cell debris that are taken up by the cell by endocytosis. As extracellular vesicles are derived from cytoplasm and cellular membranes, it is difficult to distinguish their contents from the cell using conventional reporters[14].

We tested whether the degron-tagged PH reporter could be used to specifically label and track microvesicles released *in vivo*. Microvesicles are 90-500 nm vesicles that arise from plasma membrane budding, also called ectocytosis[7]. In wild type *C. elegans* embryos, microvesicles are difficult to detect using light microscopy due to their low abundance and proximity to the plasma membrane. Microvesicle budding is normally inhibited by the TAT-5 lipid flippase, resulting in increased microvesicle release when *tat-5* is knocked down[15]. Therefore, we compared the localization of mCh::PH and mCh::PH::ZF1 after *tat-5* RNAi treatment. In mCh::PH embryos, microvesicle release is visible as thickened membrane labelling between cells (Fig. 1H-J) in comparison to control embryos (Fig. 1A-C). However, small patches of microvesicles are difficult to detect over the background of the plasma membrane fluorescence. In contrast, released microvesicles are clearly visible using the mCh::PH::ZF1 reporter (Fig. 1L-M)[3], due to proteasomal degradation of the plasma membrane label (Fig. 1N). Released extracellular vesicles are also visible moving in the fluid around cells in the space between the *tat-5* RNAi-treated embryo and the eggshell (Video 1). Thus, using a general plasma membrane reporter with a degron tag, it is possible to observe microvesicles and their movement *in vivo*.

We also tested whether it was possible to label extracellular vesicles by degron-tagging transmembrane proteins. In contrast to the proteasomal degradation of cytosolic proteins, ubiquitination of transmembrane proteins leads to endocytosis and lysosomal degradation[9]. The syntaxin SYX-4 is a single-pass transmembrane protein that localizes to the plasma membrane and endocytic vesicles (Fig. S2A-C)[16]. Degron-tagged GFP::ZF1::SYX-4 shows a similar localization before the onset of ZIF-1 expression (Fig. S2D), after which GFP::ZF1::SYX-4 is lost from the plasma membrane and accumulates in intracellular vesicles (Fig. S2E). These vesicles eventually disappear from ZIF-1-expressing cells (Fig. S2F), consistent with ubiquitin-driven endocytosis and lysosomal degradation (Fig. S2I). To test whether lysosomal degradation of a transmembrane protein can also be used to label extracellular vesicles, we treated the GFP::ZF1::SYX-4 reporter strain with *tat-5* RNAi to induce microvesicle release. Similar to the degron-tagged PH reporter (Fig. 1K-N), GFP::ZF1::SYX-4 accumulates around cells after *tat-5* knockdown (Fig. S2G-H)[15]. Thus, both membrane-associated and transmembrane proteins can be tagged with degrons to specifically label extracellular vesicles.

Degron reporters enable tracking of phagocytosed cargo

To test whether degron tags facilitate the long-term tracking of labelled objects, we chose to observe the two polar bodies in which ZF1 degradation does not occur (Fig. 1D-F). As polar bodies are dying cells, they have a nucleus and can be tagged with chromosome reporters like histone H2B, in addition to the PH domain[13]. Both polar bodies are initially found on the anterior surface of the embryo (Fig. 2A, D). The first polar body is trapped in the eggshell[17], while the second polar body (2PB) is phagocytosed by one of the anterior cells[13]. Because mCh::H2B labels all nuclei in the embryo, it can be challenging to track the 2PB phagosome among the many dividing nuclei (Fig. 2B-C, Video 2). In contrast, the degron-tagged ZF1::mCh::H2B reporter disappears sequentially from somatic nuclei, leaving the two polar bodies as the only fluorescent objects on the anterior half of the embryo (Fig 2E, Video 2). This confirms that the intervening cell and phagosome membranes protect ZF1-tagged proteins from proteasomal degradation (Fig. 2G). Improving the signal-to-noise ratio with degron tagging also improves automated tracking of the 2PB by removing overlapping traces (Fig. 2C, F). Tubulation of the 2PB phagosome into smaller vesicles can also be easily followed with degron-tagged reporters (video 1, left)[13]. Thus, degron tagging facilitates tracking and reveals organelle dynamics by removing background labelling.

Degron reporters reveal membrane topology and dynamics

In addition to facilitating tracking of labelled phagosome cargo, degron tagging also allows the specific labelling of a single membrane or surface of a membrane. Using light microscopy, it is difficult to distinguish the signal of the corpse plasma membrane from the engulfing phagosome membrane, due to their close proximity[18,19]. Using degron reporters, this can be achieved *in vivo* by degrading the reporter localized to the phagosome membrane, leaving only the corpse membrane labelled (Fig. 3B). For example, the 2PB membrane initially appears as a hollow sphere in an unlabelled cell using the degron-tagged mCh::PH::ZF1 reporter (Fig. 3A). However, the plasma membrane of the polar body corpse must be disrupted in order to degrade or recycle corpse contents within the safety of the phagosome membrane[20]. Corpse membrane breakdown can be visualized using the mCh::PH::ZF1 reporter, which is seen dispersing throughout the phagosome lumen (Fig. 3A')[13]. Thus, by removing fluorescent reporters from membrane surfaces facing the cytosol, degron-tagging enables examination of specific membranes and their dynamics.

In addition to plasma membrane and endosomal proteins, degron tagging can also be used to assess the topology of proteins associated with the nucleus. We degron-tagged the nuclear lamin LMN-1 to examine the dynamics of the nuclear cortex during cell division[21]. Similar to proteins protected by a vesicle membrane, LMN-1 is largely protected from ZF1-

mediated proteasomal degradation by the nuclear envelope (Fig. 4I) and appears as a hollow sphere during interphase (Fig. 4A). During mitosis, the nuclear envelope breaks down for chromosome segregation[22], which also allows ZIF-1 to target degron-tagged nuclear proteins (Fig. 4J). During division of ZIF-1-expressing anterior cells, an mKate2::ZF1::LMN-1 reporter is degraded from anterior nuclei (Fig. 4C, video 3), disappearing by the time nuclear envelope breakdown is visible by DIC (Fig. 4D, H). Thus, degron-tagging is a probe for membrane topology that can be used to investigate the dynamics of nuclear envelope breakdown.

Degron tagging can also reveal information on protein import/export across membranes. Nuclear lamins are translated in the cytosol and imported into the nucleus, where they integrate into the nuclear matrix[23]. Prior to the onset of ZF1-mediated degradation, the fluorescence intensity of the mKate2::ZF1::LMN-1 reporter is comparable between the anterior and posterior nuclei (Fig. 4A). After ZIF-1 expression begins in the two anterior daughter cells, the interphase levels of mKate2::ZF1::LMN-1 gradually drop in comparison to the ventral and posterior cells, where ZIF-1 is not expressed (Fig. 4B, K). This mild decrease is significantly slower than the rapid drop in fluorescence during mitosis (Fig. 4C-D, K) and suggests that a pool of mKate2::ZF1::LMN-1 is accessible to ZIF-1 during interphase. Thus, quantification of degron-tagged reporters can be a sensitive tool to examine protein dynamics in addition to organelle dynamics.

Degron reporters reveal membrane topology during abscission

In order to understand how degrons in restricted spaces can be ubiquitinated and degraded, we applied degron tagging to the process of abscission. During cell division, the actomyosin furrow closes around the spindle midbody to form a narrow intercellular bridge[24]. Both sides of the bridge are cleaved during abscission to release a ~1 μm extracellular vesicle called the midbody remnant, which is later phagocytosed (Fig. 5H)[25]. The intercellular bridge no longer permits diffusion between cells ~4 minutes after furrow ingression[24], but the first cut for abscission does not occur until ~10 minutes after furrow ingression[26]. Therefore, we asked when the actomyosin accumulated in the intercellular bridge was accessible for proteasomal degradation. We degron-tagged non-muscle myosin (NMY-2) and measured the fluorescence intensity of NMY-2::GFP::ZF1 in the bridge between the anterior daughter cells (Fig. 5A)[25]. Degradation of cytoplasmic NMY-2::GFP::ZF1 was first visible 8 ± 1 minutes after furrow ingression. NMY-2::GFP::ZF1 in the bridge showed a small but significant decline for the next 2 minutes (Fig. 5G), suggesting that NMY-2 is normally able to diffuse out of the bridge up to 10 minutes after furrow ingression. Subsequently, NMY-2::GFP::ZF1 in the bridge was protected from proteasomal degradation (Fig. 5B, G), suggesting that either a diffusion barrier had formed or abscission had occurred. Thus, we could confirm the timing of abscission

estimated from electron microscopy data from fixed embryos using degron reporters and light microscopy on living embryos.

To test whether degron tagging was able to detect novel phenotypes in abscission mutants, we depleted proteins implicated in abscission, including the ESCRT-I subunit TSG-101 and the septin UNC-59. At the onset of ZF1-mediated degradation, NMY-2::GFP::ZF1 labelled intercellular bridges in *tsg-101* or *unc-59* mutants normally (Fig. 5C, E). In contrast to control embryos where NMY-2::GFP::ZF1 fluorescence persisted through midbody release and phagocytosis (Fig. 5B), NMY-2::GFP::ZF1 fluorescence intensity continued to drop significantly in the bridge of both *tsg-101* and *unc-59* mutants (Fig. 5D, F-G), and this drop was dependent on ZIF-1 expression[25]. Phagocytosis of the midbody remnant was also delayed in both *tsg-101* and *unc-59* mutants (Fig. 5D, F)[24,25], consistent with a delay in abscission. These findings demonstrate that NMY-2 is able to diffuse out of the bridge and be degraded when abscission is delayed (Fig. 5I). As no defect was detected for *tsg-101* knockdown using a dextran diffusion assay[24], our ability to detect a defect in abscission demonstrates how highly sensitive degron tagging assays can be.

Discussion

In summary, degron-mediated degradation is more than a loss-of-function technique; it is a powerful tool to study dynamics from the level of proteins to organelles to cells. By removing the cytoplasmic fluorescence, degron tags improve the visibility of extracellular, luminal, or nuclear reporters and enable long-term tracking. Degron-tagged reporters also reveal insights with a standard epifluorescence microscope thought to be limited to super-resolution or electron microscopy on fixed samples. Our studies have focused on objects that are protected by membrane bilayers, but this approach should work for any structure resistant to ubiquitination or diffusion. Thus, degron tagging is an important addition to the cell biologist's toolbox.

As degron-tags are widely used in cell extracts, cell culture and *in vivo,* our approach can help to visualize objects in many experimental systems. We chose ZIF-1-mediated degradation of ZF1 degrons for its simplicity, because it only required the expression of a degron-tagged reporter in *C. elegans* embryos. A variation on this technique expressing a GFP nanobody fused to the ubiquitin ligase adapter ZIF-1 enables spatial control of degradation of any GFP-tagged protein in *C. elegans* at any stage[27]. Ubiquitin-mediated degradation can also be regulated by small molecule drugs, temperature, or light[8], offering many modalities to control the timing of protein degradation. Auxin-inducible degradation (AID) is a powerful option used in mammalian cultured cells and assorted animal models[28,29]. AID requires the co-expression of the degron-tagged construct with a ubiquitin ligase subunit, plus the addition of a plant hormone. This combinatorial approach enables both temporal and spatial control of

degradation. Thus, degron tagging can readily be applied to probe cell biology in many model systems.

We used degron tags to label and track objects for which conventional reporters are insufficient. For example, extracellular vesicles are typically detected by the tetraspanin proteins on their surface, but tetraspanin content is heterogeneous among extracellular vesicle subpopulations[30]. By degron-tagging membrane-associated or transmembrane proteins, we were able to specifically label extracellular vesicles *in vivo*, which has proved to be a valuable tool to screen for new regulators of extracellular vesicle budding[3]. Although our PH::ZF1 reporter is likely to favour plasma membrane-derived extracellular vesicles (microvesicles), it is possible to target endosome-derived extracellular vesicles (exosomes) by degron-tagging proteins associated with the endosome surface or by degron-tagging transmembrane proteins, given that ubiquitination drives endocytosis of transmembrane proteins (Fig. S2I). Degron-tagging reporters found at both the plasma membrane and endosome surface, such as actin-binding proteins, should label both microvesicles and exosomes[31]. Thus, degron-tagged reporters are a novel approach to label and track extracellular vesicles *in vivo* and beyond, which will enable further studies into their function.

Wide-field light microscopy is normally limited to detecting objects that are >200 nm away from each other[32]. At this resolution, neighbouring membranes cannot be distinguished. In addition to specifically labelling extracellular vesicles next to the plasma membrane, we showed that degron-tagged reporters could distinguish the cargo corpse membrane from the engulfing phagosome membrane. This enabled the visualization of corpse membrane dynamics during phagolysosomal clearance using wide-field microscopy[13]. These reporters enable the precise staging of phagosomes for approaches such as correlative light and electron microscopy (CLEM)[33], which can be used to determine the ultrastructure of membrane breakdown during phagolysosomal clearance. Therefore, degron-tagging is a useful tool to reveal novel insights into organelle dynamics in addition to the long-term tracking of specific cells *in vivo*.

The limited resolution of wide-field microscopy also prevents the observation of membrane fusion and fission events, including during cell division. Using a degron-tagged reporter, we were able to measure early changes in the topology of the nuclear envelope as well as in the restricted space of the intercellular bridge, which was previously only possible using electron microscopy[26]. We were also able to detect defects in abscission after knocking down an ESCRT subunit[25], which were not visible using cytosolic diffusion assays[24]. Degron tagging is therefore a sensitive tool to study the topology of membranes while they undergo fusion or fission.

Degron tagging also revealed protein dynamics and topology. Knocking down septins or TSG-101 led to distinct rates of degron-mediated degradation of the myosin reporter, which could indicate that the intercellular bridge is open to differing degrees in these mutants,

resulting in different rates of diffusion out of the bridge. We also found that a pool of the degron-tagged lamin reporter underwent degradation during interphase. As ubiquitination can lead to nuclear export through nuclear pore complexes[34], this may indicate that the degron is ubiquitinated in the nucleus during interphase, which leads to export of the reporter into the cytosol, where it is then accessible for proteasomal degradation. Alternatively, this may be due to the activity of the nuclear proteasome[35]. As degradation of a reporter depends on its location within the cell, the degron approach can potentially be applied to determining the topology of transmembrane proteins (type I/II) or to distinguish cytosolic from luminal proteins. Thus, degron tags can be used to analyse protein import/export into organelles and determine the topology of proteins associated with membrane-bound organelles. In summary, degron tagging improves the signal-to-noise ratio, reveals super-resolution insights on a standard microscope, and provides insights into localization and dynamics from the level of cells to proteins.

Acknowledgements

Michaela Geisenhof assisted with measurements, and the imaging facility of the Rudolf Virchow Center provided OriginPro software and assistance with calculations. Strains and reagents were provided by Peter Askjaer, Zhirong Bao, Michael Glotzer, Jeremy Nance, Christian Pohl, and the *Caenorhabditis* Genetics Center (CGC), which is funded by NIH Office of Research Infrastructure Programs (P40 OD010440). This work was funded by the Rudolf Virchow Center and Deutsche Forschungsgemeinschaft (DFG) grant WE 5719/2-1 to AMW. We thank Katrin Heinze, Sonja Lorenz, and Anna Liess for critical reading of this manuscript.

Author contributions

AMW conceived and designed the study. KBB, GF, LI, and AMW performed and interpreted experiments. KBB, GF, and AMW wrote the manuscript.

Competing Interests

The authors declare no competing interests.

Materials and methods

Worm strains and maintenance

Caenorhabditis elegans strains were maintained according to standard protocol at room temperature[36]. For a list of strains used in this study, see Table S1. *unc-59* loss-of-function mutant embryos were generated by feeding *unc-59* RNAi to the WEH132 strain bearing a hypomorphic *unc-59* mutation[25].

Worm transformation

FT205, WEH251, and WEH399 were made by biolistic transformation using a Bio-Rad PDS-1000, as described[37]. The DP38 strain was bombarded with MP322 (gift of Michael Glotzer[15]) to generate FT205. WEH251 was generated by co-bombardment of pGF04[13] and pJN254 (gift of Jeremy Nance[38]) into the HT1593 strain. HT1593 was bombarded with pGF13[13] to generate WEH399.

RNAi experiments

RNA interference (RNAi) was performed by feeding double-stranded RNA (dsRNA)-expressing bacteria from the L1 larval stage through adulthood at 25˚C (60-70 hours) according to established protocols[39]. The following RNAi clones were used from available libraries (Source BioScience): *tat-5* (JA:F36H2.1) and *unc-59* (mv_W09C5.2). The RNAi clone for *tsg-101* was designed according to the Cenix clone 49-f7[40] and dsRNA was transcribed, as described[25]. 1 mg/ml *tsg-101* dsRNA was injected into the gonad of young adult worms 20-26h before analysis. Efficiency of *tsg-101* RNAi was judged by a mild delay in internalization of the AB midbody.

Light Microscopy

Embryos were dissected from gravid adults and mounted in M9 buffer on an agarose pad on a glass slide. For FT205 and FT368, imaging was performed using a Zeiss AxioImager, 40X 1.3 NA objective, an Axiocam MRM camera, and AxioVision software, as described previously[15]. For WEH02, WEH51, WEH132, and WEH142, Z-stacks were acquired sequentially for GFP and mCherry every 20 seconds, as described[25]. For strains WEH260 and WEH296, Z-stacks were acquired for mCherry every minute at room temperature, as described[13]. For WEH251, Z-stacks were acquired for mCherry every 20 seconds using a Leica DM5500 wide-field fluorescence microscope with a HC PL APO 40X 1.3 NA oil objective lens supplemented with a Leica DFC365 FX CCD camera controlled by LAS AF software. For WEH399, Z-stacks were acquired for mKate2 and DIC every 30 seconds. Time-lapse series were analysed using Imaris (Bitplane).

Cell cycle timing

To compare the speed of development between control and ZF1-tagged strains, the time from the 6- to the 12- and to the 24-cell stages (one and two subsequent cell cycles in the AB lineage) were calculated from time-lapse series. The cell cycle time was measured from the ingression of any furrow in the two ABx cells to the ingression of any furrow in the four ABxx or eight ABxxx cells. To estimate percent changes, we compared the timing of ABx division to ABxx division for reporter strains with and without the ZF1 degron.

Tracking

H2B-labeled nuclei were tracked over time using the surface function of Imaris with thresholding to define objects.

Quantification of corpse membrane breakdown

Corpse membrane topology was measured using a box scan across the 2PB phagosome in the WEH260 strain. A box with 3-pixel thickness was drawn through the middle of the phagosome using Fiji (NIH) and the mean profile intensity was measured.

Fluorescence intensity measurements

Mean fluorescence intensity of the LMN-1 reporter (Fig. 4K) was measured in a circle with an area of 0.8 μm^2 using ImageJ (NIH) in ABp and EMS nuclei. Fluorescence intensity was measured from the first time point that EMS nucleus reformed in a round shape after P1 division until the LMN-1 marker in ABp nucleus was not distinguishable from the cytoplasm. Fluorescence intensity of the EMS nucleus was measured as an internal control. Data are reported as the ratio of the fluorescence intensity of the ABp nucleus to that of the EMS nucleus. A sigmoidal decay curve with tilted baseline was fitted to the data using OriginPro (OriginLab) and the slopes of the initial mild fluorescence loss during interphase and the sharp drop during mitosis were calculated.

Mean fluorescence intensity of the NMY-2::GFP::ZF1 reporter (Fig. 5G) was measured in a circle with an area of 0.5 μm^2 using ImageJ (NIH), as described previously[25]. Midbody fluorescence was measured from contractile ring closure until the end of the time lapse series or until the midbody was not distinguishable from the cytoplasm. Fluorescence intensity of the first polar body was measured as an internal control. An exponential decay curve was fit to the polar body data using OriginPro and used to correct for fluorescence loss due to photobleaching. Embryos were excluded if the P0 and AB midbodies were too close to each other or if the polar body data did not fit an exponential decay function. NMY-2 data are reported as the ratio of the fluorescence intensity of the midbody to the expected value of the polar body after cytoplasmic background subtraction. Timing of the onset of degradation of NMY-2::GFP::ZF1 in the

cytoplasm was judged by eye by comparing the relative brightness of ABp and EMS using Imaris.

Image Processing

For clarity, images were rotated, colorized and the intensity was adjusted using Adobe Photoshop. All images show a single optical section (Z), except for Fig. 2 and Fig. S2. In Fig. 2, six Zs with 1.2 μm steps were maximum projected using Leica LAS X software. In Fig. S2, images where maximum projected to span a region of 2.5 μm using Fiji (NIH). Fig. 2C, 2F, and videos were rotated, colorized, and the intensity was adjusted using Imaris. Several Zs were maximum projected in Imaris for videos. For video 3, the brightness was adjusted in each frame using Photoshop to compensate for photobleaching.

Statistical evaluation

Student's one-tailed *t*-test was used to test statistical significance. When necessary, Bonferroni correction was used to adjust for multiple comparisons.

Fig. 1

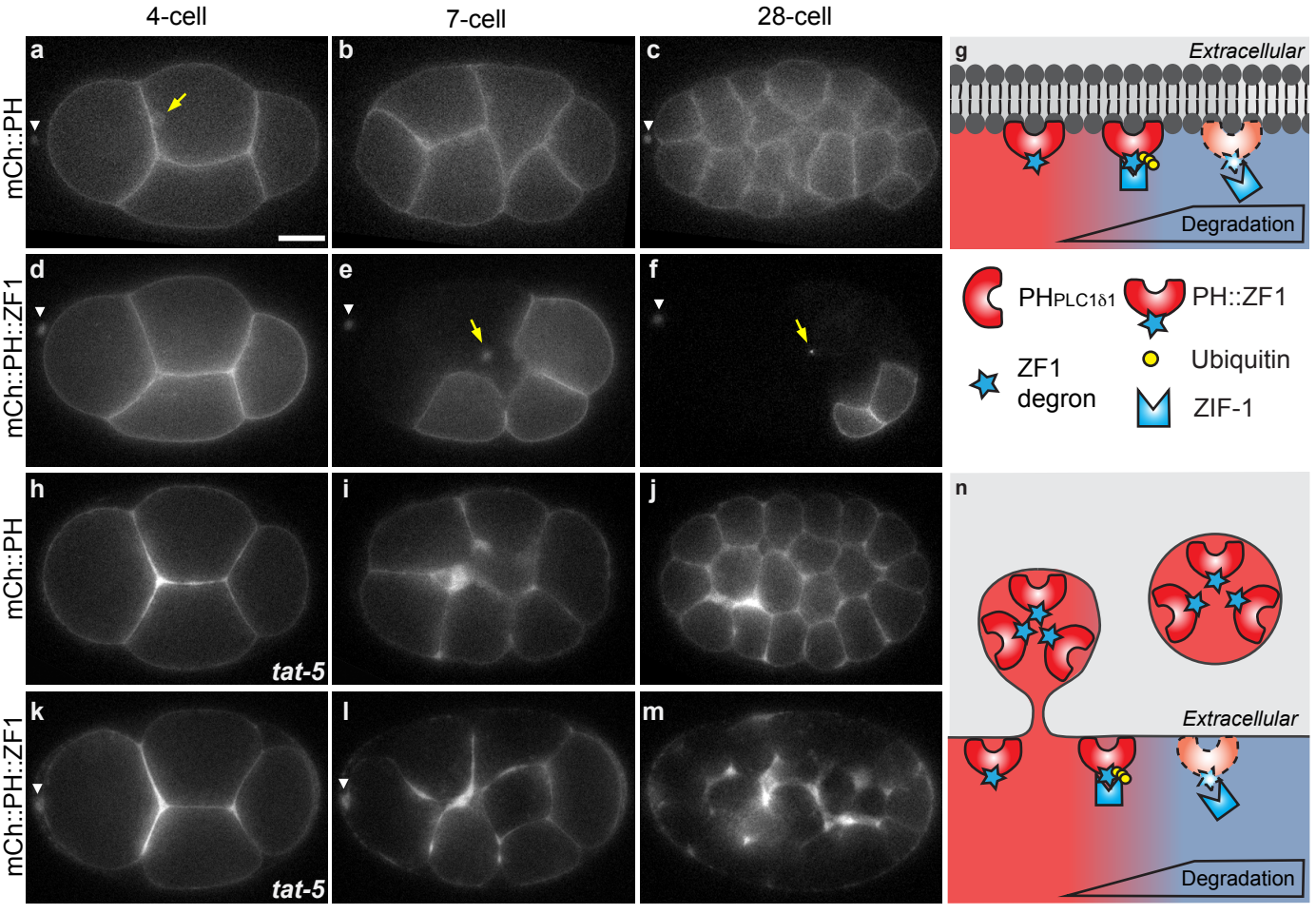
4-cell
7-cell
28-cell
mCh::PH
mCh::PH::ZF1
mCh::PH
mCh::PH::ZF1
a
b
c
d
e
f
h
i
j
k
l
m
tat-5
tat-5
g
Extracellular
Degradation
PHPLC1δ1
PH::ZF1
ZF1 degron
Ubiquitin
ZIF-1
n
Extracellular
Degradation

Fig. 2

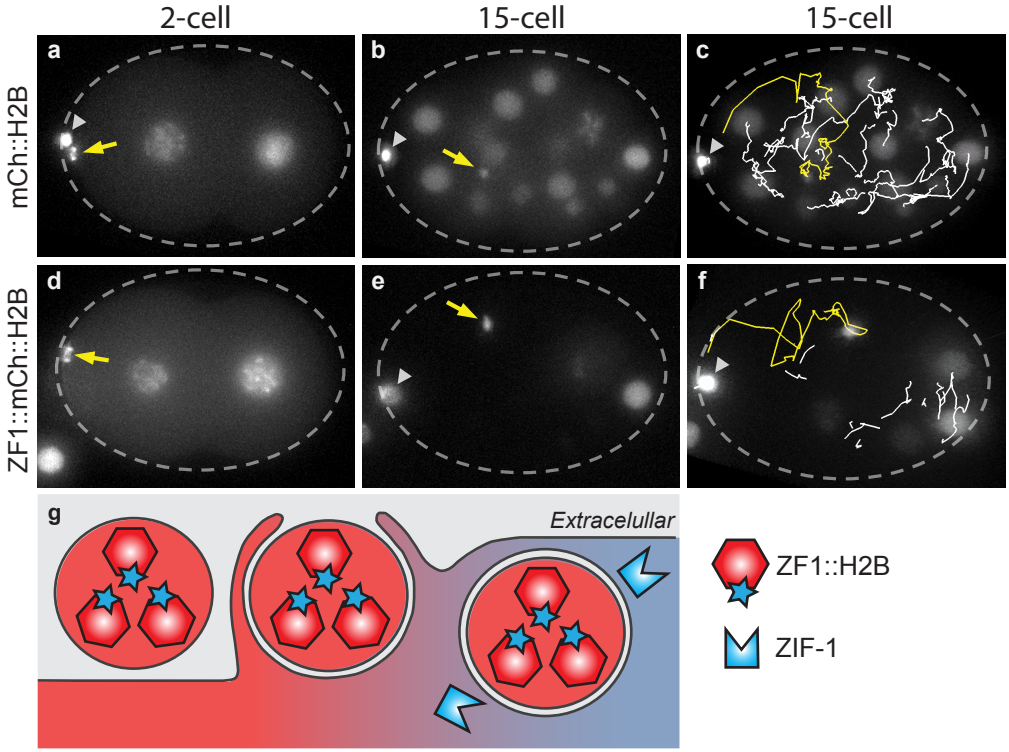
2-cell
15-cell
15-cell
mCh::H2B
ZF1::mCh::H2B
a
b
c
d
e
f
g
Extracelullar
ZF1::H2B
ZIF-1

Fig. 3

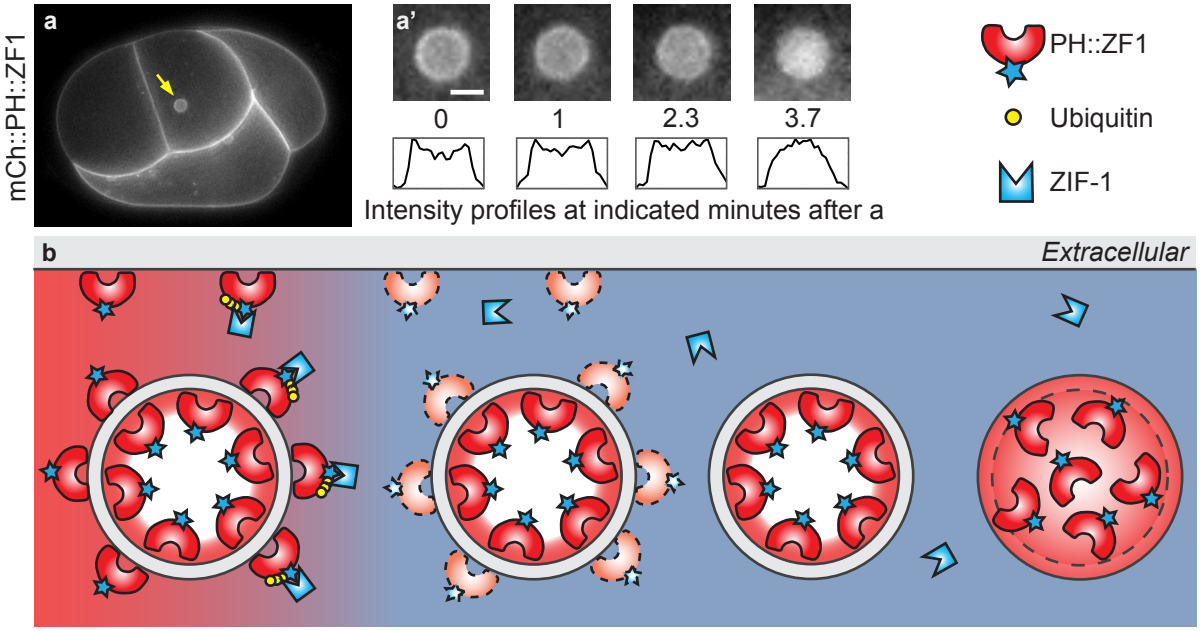
mCh::PH::ZF1
a
a'
0
1
2.3
3.7
Intensity profiles at indicated minutes after a
PH::ZF1
Ubiquitin
ZIF-1
b
Extracellular

Fig. 4

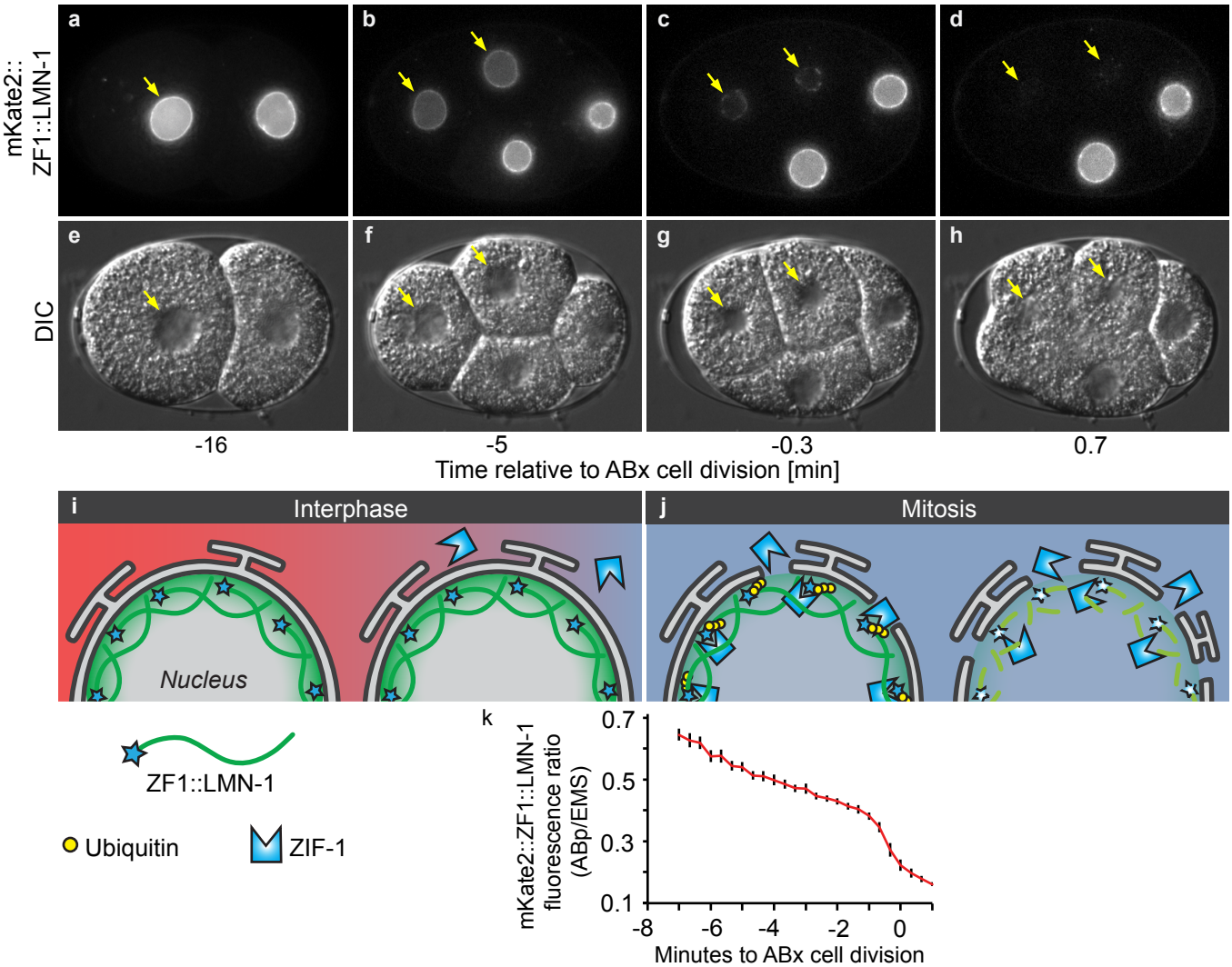
mKate2::
ZF1::LMN-1
DIC
a
b
c
d
e
f
g
h
-16
-5
-0.3
0.7
Time relative to ABx cell division [min]
i
Interphase
j
Mitosis
Nucleus
ZF1::LMN-1
Ubiquitin
ZIF-1
k
mKate2::ZF1::LMN-1
fluorescence ratio
(ABp/EMS)
0.7
0.5
0.3
0.1
-8
-6
-4
-2
0
Minutes to ABx cell division

Fig. 5

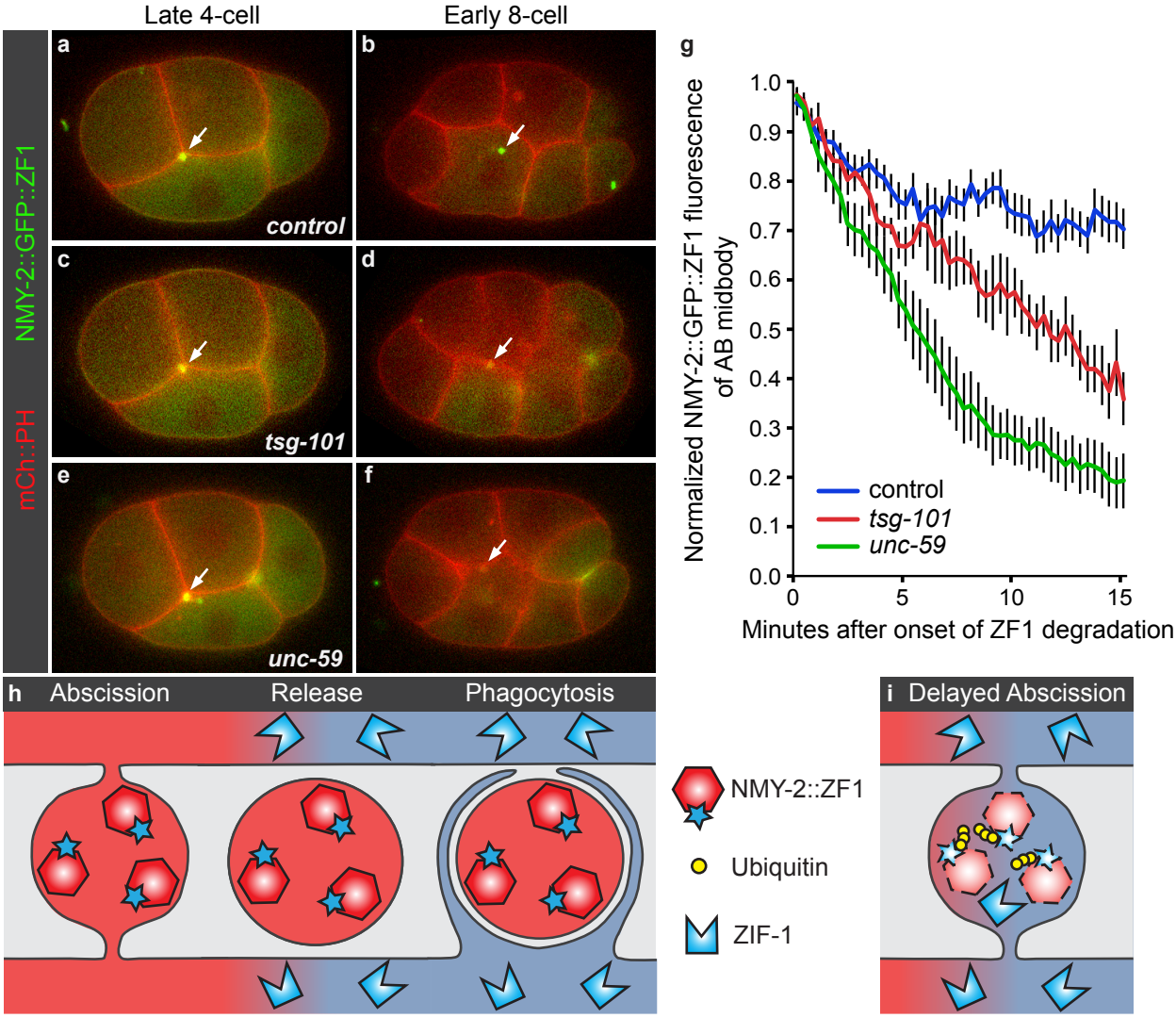
Late 4-cell
Early 8-cell
NMY-2::GFP::ZF1
mCh::PH
a
b
c
d
e
f
control
tsg-101
unc-59
g
Normalized NMY-2::GFP::ZF1 fluorescence of AB midbody
1.0
0.9
0.8
0.7
0.6
0.5
0.4
0.3
0.2
0.1
0.0
0
5
10
15
Minutes after onset of ZF1 degradation
control
tsg-101
unc-59
h
Abscission
Release
Phagocytosis
NMY-2::ZF1
Ubiquitin
ZIF-1
i
Delayed Abscission

Figure legends

Fig. 1: The ZF1 degron enables labelling of specific cells and vesicles in *C. elegans* embryos. A-C) The lipid-binding mCh::$PH_{PLC1\partial1}$ reporter localizes to the plasma membrane and endocytic vesicles (arrow) in 4-, 7-, and 28-cell embryos. D-F) ZIF-1-driven proteasomal degradation of the degron-tagged mCh::$PH_{PLC1\partial1}$::ZF1 reporter starts in anterior blastomere (AB) cells during the 4-cell stage (D), leading to the absence of the mCh::PH::ZF1 fluorescence in anterior AB cells at the 7-cell stage (E) and most somatic cells at the 28-cell stage (F). The ubiquitin ligase adapter ZIF-1 is not expressed in the posterior germ line or in anterior polar bodies (arrowhead), resulting in the persistence of mCh::PH::ZF1 in these cells. Arrows indicate labelled intracellular vesicles, which are protected from proteasomal degradation by intervening membranes. See also video 1. Anterior is left, dorsal is up. Scale bar: 10 µm. G) The lipid-binding PH domain tagged with the ZF1 degron is recognized by the ubiquitin ligase adaptor ZIF-1 and ubiquitinated. Polyubiquitination leads to proteasomal degradation of degron-tagged fluorescent reporters (dotted lines). H-J) Embryos treated with *tat-5* RNAi show increased mCh::PH membrane labelling due to accumulated microvesicles at the 4-, 7-, and 28-cell stage. K) Increased mCh::PH::ZF1 is visible at the 4-cell stage in embryos treated with *tat-5* RNAi. L-M) Gradual degradation of mCh::PH::ZF1 in somatic cells facilitates visualization of released microvesicles in a 7- and 28-cell embryo. Due to degradation of cytosolic mCh::PH::ZF1 reporter at the plasma membrane, even small amounts of released microvesicles are easily visible. See also video 1. N) Degron-tagged PH domain reporters are released in extracellular vesicles that bud from the plasma membrane before ZIF-1 expression. ZIF-1 expression leads to the ubiquitination and proteasomal degradation of cytosolic ZF1-tagged reporters (dotted lines). ZF1-tagged membrane reporters in released vesicles are not ubiquitinated or degraded and maintain fluorescence.

Fig. 2: Degron reporters label phagocytosed cell debris and enable tracking.
A-C) The histone reporter mCh::H2B labels chromosomes in embryonic nuclei and two polar bodies. The first polar body (arrowhead) is trapped in the eggshell (dashed oval). A) The second polar body (2PB, arrow) neighbours the anterior blastomere (AB cell) in a 2-cell embryo. B) The 2PB is engulfed in a phagosome in a 15-cell embryo. Due to H2B fluorescence from surrounding embryonic nuclei, it is hard to track the 2PB. C) Automated tracking of the 2PB (yellow) results in crossing tracks from nearby nuclei (white), increasing the potential need for manual correction. D-F) Embryos labelled with ZF1-tagged mCh::H2B. D) Released 2PB neighbours a 2-cell embryo. E) After engulfment, 2PB is easily trackable due to degradation of ZF1::mCh::H2B in somatic cell nuclei. See also video 2. F) Automated tracking of the 2PB (yellow) is simplified by removing the label of nearby nuclei (white). G) Degron reporters

released in cells or other debris prior to expression of the ZIF-1 ubiquitin ligase adapter are protected from ZF1-mediated degradation. After engulfment in a second layer of membrane, they are still protected from proteasomal degradation. As degron reporters are degraded in the cytosol, only the reporters within the phagosome remain fluorescent, improving the signal-to-noise ratio.

Fig. 3: Degron reporters label specific membranes.
A) The mCh::PH::ZF1 reporter labels the plasma membrane of embryonic cells and of the phagocytosed second polar body (2PB) (arrow) in a 6-cell embryo. ZF1-mediated degradation in anterior cells degrades the reporter from the plasma membrane as well as on the phagosome surface, but the 2PB plasma membrane remains labelled. A') Several minutes after phagocytosis, the 2PB plasma membrane breaks down inside the phagolysosome and the reporter gradually disperses throughout the phagolysosome lumen, as demonstrated by line scans through the phagolysosome (time between insets is indicated in minutes). Scale bar is 2 µm. B) PH::ZF1 reporters on the phagosome membrane are accessible to proteasomal degradation, while PH::ZF1 reporters inside the corpse membrane are protected. Model of membrane breakdown inside the phagolysosome, demonstrating the shape change from a hollow to a filled sphere.

Fig. 4: Degron reporters reveal nuclear envelope topology during cell division.
A) Prior to ZIF-1 expression, mKate2::ZF1::LMN-1 is similarly bright in the nuclear matrix of the anterior AB cell and the posterior cell. B) After the onset of ZIF-1 expression in anterior daughter cells (ABx), mKate2::ZF1::LMN-1 starts to lose fluorescence in anterior cells, suggesting it is shuttled between the cytosol and nucleus. C-D) During mitosis, the nuclear envelope is disassembled, leading to rapid proteasomal degradation of mKate2::ZF1::LMN-1. See also video 3. E-H) DIC images show nuclear morphology during cell cycle progression. I) During interphase, the nuclear envelope is intact, hindering ZIF-1 binding to ZF1-tagged reporters inside the nuclear envelope. J) During mitosis, the nuclear envelope is remodelled into the endoplasmic reticulum, allowing binding of ZIF-1 to ZF1-tagged reporters, which leads to ubiquitination and rapid proteasomal degradation. K) Quantification of mKate2::ZF1::LMN-1 fluorescence in the dorsal ABp nucleus compared to the ventral EMS nucleus. The slow decline in the intensity of mKate2::ZF1::LMN-1 during interphase reflects the degradation of mKate2::ZF1::LMN-1 in the cytoplasm. The fluorescence drops two orders of magnitude faster during ABx cell division (time 0, $n=7$, $p<0.005$), when breakdown of the nuclear envelope gives ZIF-1 and/or the proteasome full access to mKate2::ZF1::LMN-1.

Fig. 5: Degron reporters reveal membrane topology during abscission.

A-F) Time-lapse images of embryos expressing mCh::PH to label the plasma membrane and NMY-2::GFP::ZF1 to label non-muscle myosin in the cytokinetic ring. A) In a control embryo, NMY-2::GFP::ZF1 between the anterior daughter cells (arrow) is protected from ZF1-mediated degradation due its release outside cells in the midbody remnant after abscission. B) NMY-2::GFP::ZF1 in the phagocytosed midbody remnant is protected from proteasomal degradation by engulfing membranes. C) In embryos depleted of the ESCRT-I subunit TSG-101, NMY-2::GFP::ZF1 localizes to the intercellular bridge normally. D) NMY-2::GFP::ZF1 is degraded after *tsg-101* knockdown, indicating that abscission is incomplete and NMY-2::GFP::ZF1 is accessible to the degradation machinery. Engulfment of the AB midbody is also delayed, likely due to incomplete abscission. E-F) Embryos depleted of the Septin UNC-59 show rapid degradation of NMY-2::GFP::ZF1 from the intercellular bridge and delayed engulfment of the midbody remnant due to defects in abscission. G) Fluorescence intensity of the NMY-2::GFP::ZF1 reporter on the intercellular bridge between anterior daughter cells (AB midbody). NMY-2::GFP::ZF1 fluorescence in the bridge drops significantly for two minutes after the onset of ZF1 degradation in the cytoplasm of control embryos (blue, $p<0.05$ using Student's t-test with Bonferroni correction), showing that NMY-2 is able to diffuse out of the bridge. Fluorescence then persists, showing that formation of the diffusion barrier, symmetric abscission, and engulfment protect the degron-tagged reporter from degradation. In contrast, NMY-2::GFP::ZF1 fluorescence continues to drop in *tsg-101* RNAi-treated embryos (red, $p<0.05$ compared to control after 8 min) and *unc-59* mutants (green, $p<0.05$ compared to control after 3.5 min), showing that the ZF1 degron technique is sensitive to detecting small defects in abscission. H) In control embryos, degron reporters on the intercellular bridge are protected from proteasomal degradation due to release after abscission and encapsulation in a phagosome. I) In abscission mutants, degron reporters are accessible to the cytosol, leading to their removal by proteasomal degradation.

Fig. S1

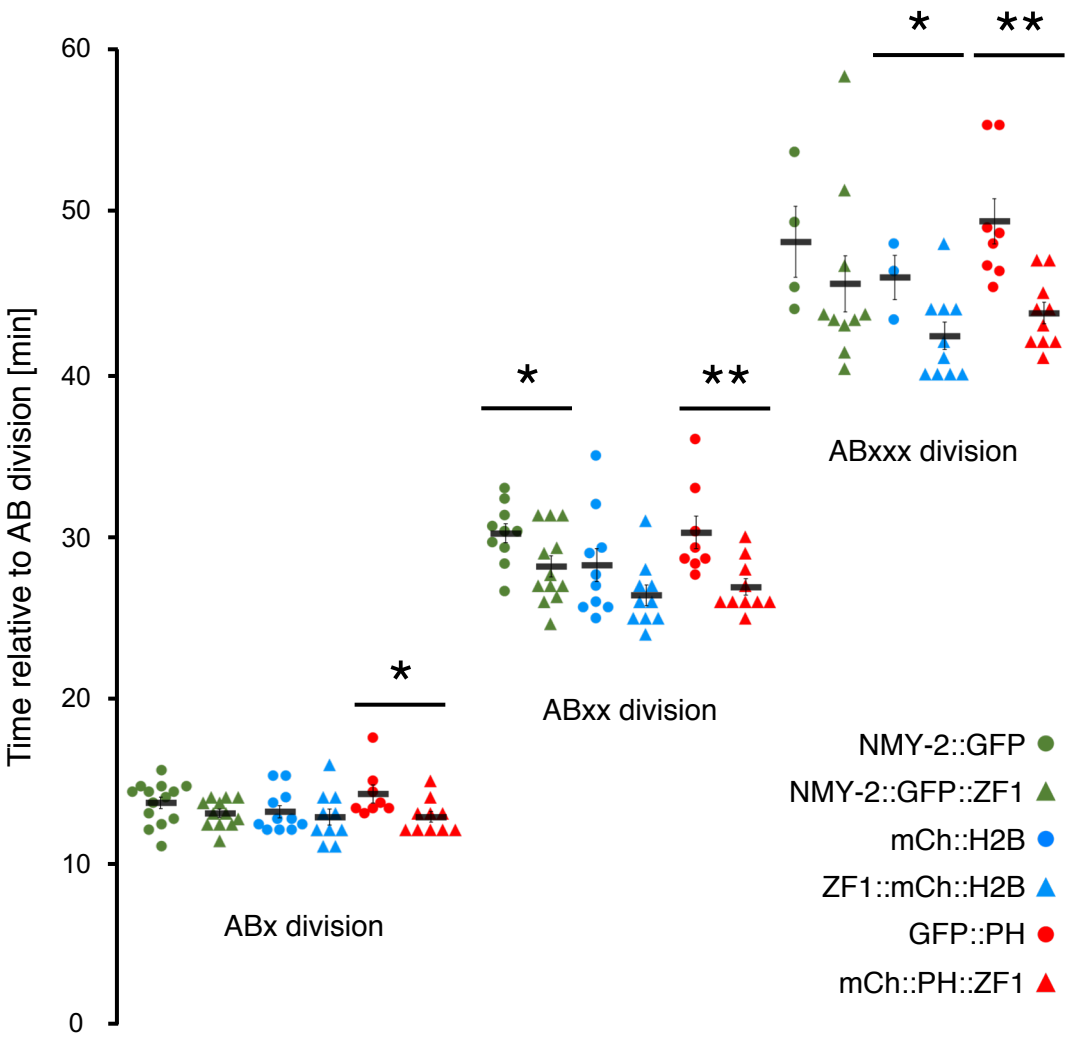
Time relative to AB division [min]
60
50
40
30
20
10
0
*
*
**
*
**
ABx division
ABxx division
ABxxx division
NMY-2::GFP
NMY-2::GFP::ZF1
mCh::H2B
ZF1::mCh::H2B
GFP::PH
mCh::PH::ZF1

Fig. S2

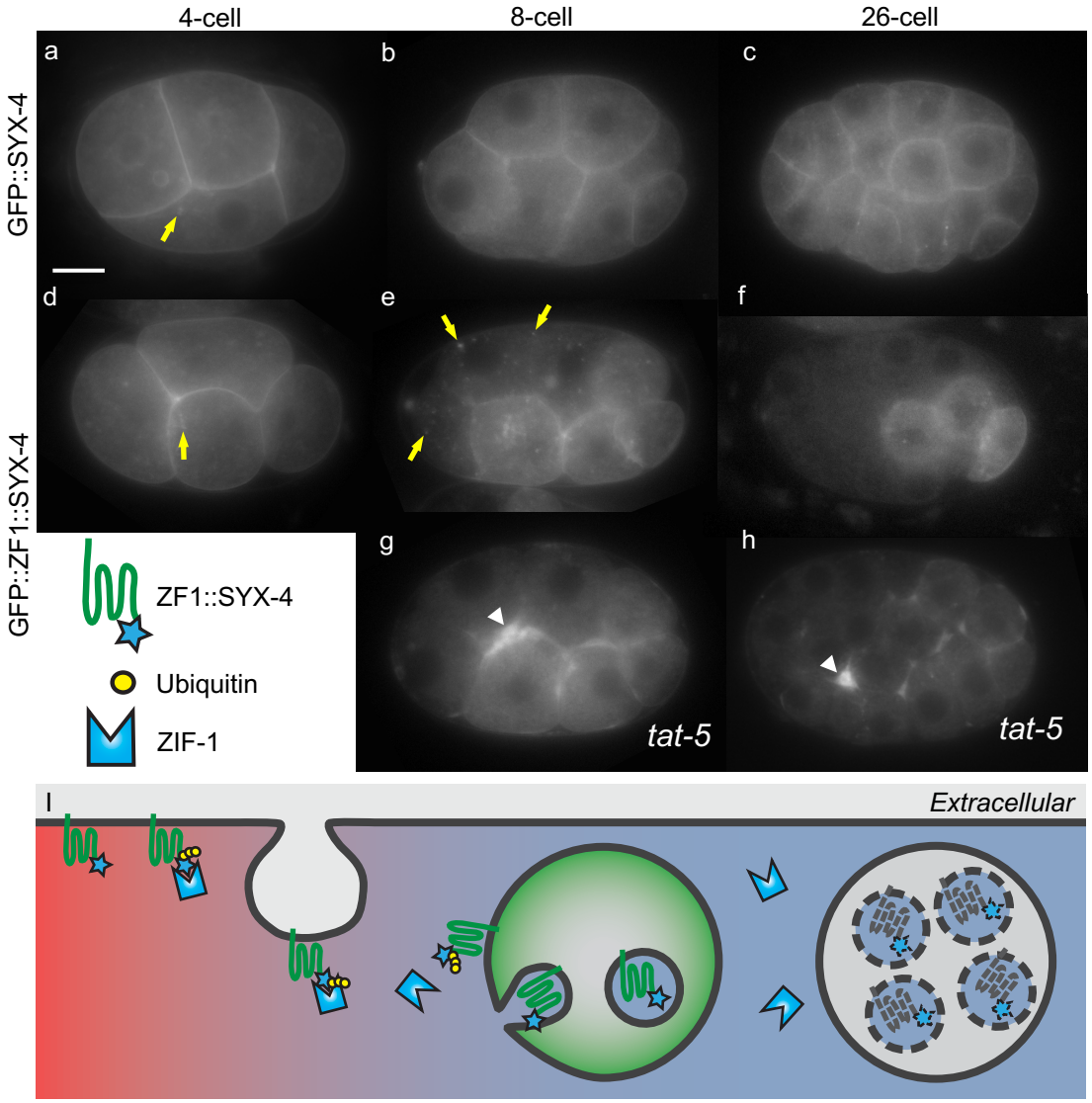
4-cell
8-cell
26-cell
GFP::SYX-4
GFP::ZF1::SYX-4
a
b
c
d
e
f
g
h
ZF1::SYX-4
Ubiquitin
ZIF-1
tat-5
tat-5
I
Extracellular

Supplemental Figure Legends

Fig. S1: The development of strains expressing degron-tagged reporters is not delayed.

The timing of subsequent divisions of the anterior AB cell were compared between control reporter strains (circles) and ZF1-tagged reporter strains (triangles), where the same protein was fluorescently-tagged with or without the ZF1 degron. Development was not delayed after ZF1-tagging non-muscle myosin NMY-2 (green), a histone H2B (blue) or the PH domain of PLC1∂1 (red). The time of the AB cell division (3-cell stage) was compared to the timing of the AB daughter (ABx, 6-cell), AB granddaughter (ABxx, 12-cell) and AB great-granddaughter (ABxxx, 24-cell) cell divisions. Division timing was slightly accelerated in ZF1-tagged strains (11% comparing ABx to ABxx division for PH strains (n=10 WEH260 vs. n=9 WEH02 embryos), 10% for H2B strains (n=10 WEH296 vs. n=10 WEH248) and 8% for NMY-2 strains (n=16 WEH51 vs. n=10 BV113)). However, some of the observed differences may reflect different imaging conditions. Both green and red time-lapse images were acquired for control PH and H2B strains, whereas their ZF1-tagged counterparts were only imaged for red fluorescence. Both NMY-2 and ZF1-tagged NMY-2 data sets were imaged for both green and red fluorescence. Bars represent mean ± SEM. *$p<0.05$, **$p<0.01$ using Student's t-test.

Fig. S2: Degron tags drive endocytosis and lysosomal degradation of a transmembrane reporter. A-C) A transmembrane syntaxin localizes to the plasma membrane and endosomes (arrow) in 4-, 8-, and 26-cell GFP::SYX-4-expressing embryos. D) Prior to ZIF-1 expression, the degron-tagged GFP::ZF1::SYX-4 reporter localizes to the plasma membrane and endosomes (arrow). E) After ZIF-1 expression starts in anterior blastomere (AB) daughter cells, GFP::ZF1::SYX-4 is endocytosed (arrows) and is no longer found in the plasma membrane. F) After endocytosis, GFP::ZF1::SYX-4 vesicles disappear from the anterior cells by the 26-cell stage, consistent with lysosomal degradation. Anterior is left, dorsal is up. G-H) Embryos treated with *tat-5* RNAi show increased GFP::ZF1::SYX-4 membrane labelling due to accumulated microvesicles (arrowhead) at the 8- and 26-cell stage. Scale bar: 10 μm. I) A transmembrane protein tagged with the ZF1 degron is recognized by the ubiquitin ligase adaptor ZIF-1 at the plasma membrane and ubiquitinated. Polyubiquitination leads to endocytosis and microautophagy, which results in degradation of reporters on intraluminal vesicles within lysosomes (dotted lines) of degron-tagged fluorescent reporters.

Video Legends

Video 1. Degron reporters facilitate detection of released extracellular vesicles

Time-lapse movies of WEH260 embryos expressing mCh::PH::ZF1 on membranes (cyan) with or without *tat-5* RNAi treatment to induce extracellular vesicle accumulation. In an untreated control embryo, mCh::PH::ZF1 localizes to the plasma membrane, but gradually disappears in somatic cells, starting with the anterior cells. In a *tat-5* RNAi-treated embryo, mCh::PH::ZF1 persists on released extracellular vesicles that accumulate between cells. mCh::PH::ZF1 persists in posterior germ cells, as well as in polar bodies in both control and *tat-5* RNAi-treated embryos. Anterior is to the left, dorsal is up. Time-lapse data were collected every minute for 90 minutes (6 fps). 9 Zs are projected with an interval of 1.2 μm.

Video 2. Degron reporters enable tracking of a phagocytosed cell corpse

Time-lapse movies of WEH142 embryos expressing mCh::H2B and WEH339 embryos expressing ZF1::mCh::H2B in nuclei, including both polar bodies (arrowheads). It is harder to follow the corpse of the second polar body labelled with mCh::H2B, due to the fluorescence of nearby nuclei. ZF1::mCh::H2B is degraded in sequential sets of somatic nuclei, facilitating tracking of the polar bodies as they remain the only fluorescent objects in the anterior half of the embryo. Anterior is to the left, dorsal is up. Time-lapse data were collected every 20 seconds for WEH142 and every 30 seconds for WEH339 for 40 minutes in total (playing at 15 fps and 10 fps, respectively). 11 Zs with 1.2 μm intervals are projected.

Video 3. Degron reporters reveal nuclear envelope dynamics during cell division

Time-lapse movie of a WEH251 embryo expressing mKate2::ZF1::LMN-1 to mark the nuclear lamina (grey). The reporter gradually loses fluorescence intensity in anterior somatic cells during interphase, followed by a sharp drop of fluorescence in dividing cells when nuclear envelope breakdown occurs. Anterior is to the left, dorsal is up. Time-lapse data were collected every 20 seconds for ~21 minutes (6 fps). 7 Zs with 1 μm intervals are projected.

Supplemental Table

Table S1: Strains used in this study.

Strain	Genotype	Source
BV113	*zuIs45[nmy-2::NMY-2::GFP + unc-119(+)] IV; zbIs2[pie-1::Lifeact::Cherry + unc-119(+)]*	Singh & Pohl 2014[41]
DP38	*unc-119(ed3) III; daf-?*	CGC
FT205	*xnIs88[MP322: syx-4::GFP::SYX-4::syx-4 3'UTR; unc-119(+)]; unc-119(ed3) III*	This study
FT368	*unc-119(ed3) III; xnIs144[syx-4::GFP::ZF1::SYX-4::syx-4 3'UTR; unc-119(+)]*	Wehman et al., 2011[15]
HT1593	*unc-119(ed3) III*	CGC
WEH02	*unc-119(ed3) III; ltIs38[pie-1::GFP::PH(PLC1∂1) + unc-119(+)]; xnIs8[pJN343: nmy-2::NMY-2::mCherry, unc-119(+)]*	Fazeli et al., 2016[25]
WEH51	*unc-119(ed3) III; xnIs65[nmy-2::gfp::zf1, unc-119(+)] IV; ltIs44[pie-1::mCherry::PH(PLC1∂1), unc-119(+)] V*	Fazeli et al., 2016[25]
WEH132	*unc-59(e261) I; unc-119(ed3) III; xnIs65[nmy-2::gfp::zf1, unc-119(+)] IV; ltIs44[pie-1::mCherry::PH(PLC1∂1), unc-119(+)] V*	Fazeli et al., 2016[25]
WEH142	*unc-119(ed3) III; zbIs1[pie-1::Lifeact::GFP; unc-119(+)]; Is[mCherry::HistoneH2B] IV*	Fazeli et al., 2018[13]
WEH248	*unc-119(ed3) III; pwIs21[pie-1::gfp::rab-7, unc-119(+)]; Is[mCherry::HistoneH2B] IV*	Fazeli et al., 2018[13]
WEH251	*unc-119(ed3) III; wurIs85[pGF04: pie-1::mKate2::ZF1::LMN-1, pJN254: unc-119(+)]*	This study
WEH260	*unc-119(ed3) III; wurIs90[pGF7: pie-1::mCherry::PH(PLC1∂1)::ZF1, unc-119(+)]*	Beer et al., 2018[3]
WEH296	*unc-119(ed3) III; +/wurIs103[pGF13: pie-1::ZF1::mCherry::his-15; unc-119(+)]*	Fazeli et al., 2018[13]
WEH399	*unc-119(ed3) III; wurIs144[pGF13: pie-1::ZF1::mCherry::his-15; unc-119(+)]*	This study

References

1. Edidin, M. Lipids on the frontier: A century of cell-membrane bilayers. *Nat. Rev. Mol. Cell Biol.* **4,** 414–418 (2003).
2. Huang, B., Babcock, H. & Zhuang, X. Breaking the diffraction barrier: Super-resolution imaging of cells. *Cell* **143,** 1047–1058 (2010).
3. Beer, K. B. *et al.* Extracellular vesicle budding is inhibited by redundant regulators of TAT-5 flippase localization and phospholipid asymmetry. *Proc. Natl. Acad. Sci.* **115,** E1127 LP-E1136 (2018).
4. Várnai, P. & Balla, T. Visualization and manipulation of phosphoinositide dynamics in live cells using engineered protein domains. *Pflugers Arch. Eur. J. Physiol.* **455,** 69–82 (2007).
5. Flannagan, R. S., Jaumouillé, V. & Grinstein, S. The Cell Biology of Phagocytosis. *Annu. Rev. Pathol. Mech. Dis.* **7,** 61–98 (2012).
6. Leung, B. O. & Chou, K. C. Review of super - Resolution fluorescence microscopy for biology. *Appl. Spectrosc.* **65,** 967–980 (2011).
7. Beer, K. B. & Wehman, A. M. Mechanisms and functions of extracellular vesicle release in vivo—What we can learn from flies and worms. *Cell Adhes. Migr.* **11,** 135–150 (2017).
8. Natsume, T. & Kanemaki, M. T. Conditional Degrons for Controlling Protein Expression at the Protein Level. *Annu. Rev. Genet.* **51,** 83–102 (2017).
9. Foot, N., Henshall, T. & Kumar, S. Ubiquitination and the Regulation of Membrane Proteins. *Physiol. Rev.* **97,** 253–281 (2017).
10. DeRenzo, C., Reese, K. J. & Seydoux, G. Exclusion of germ plasm proteins from somatic lineages by cullin-dependent degradation. *Nature* **424,** 685–689 (2003).
11. Oldenbroek, M. *et al.* Multiple RNA-binding proteins function combinatorially to control the soma-restricted expression pattern of the E3 ligase subunit ZIF-1. *Dev. Biol.* **363,** 388–398 (2012).
12. Armenti, S. T., Lohmer, L. L., Sherwood, D. R. & Nance, J. Repurposing an endogenous degradation system for rapid and targeted depletion of C. elegans proteins. *Development* **141,** 4640–4647 (2014).
13. Fazeli, G., Stetter, M., Lisack, J. N. & Wehman, A. M. C. elegans Blastomeres Clear the Corpse of the Second Polar Body by LC3-Associated Phagocytosis. *Cell Rep.* **23,** 2070–2082 (2018).
14. Van Niel, G., D'Angelo, G. & Raposo, G. Shedding light on the cell biology of extracellular vesicles. *Nat. Rev. Mol. Cell Biol.* **19,** 213–228 (2018).
15. Wehman, A. M., Poggioli, C., Schweinsberg, P., Grant, B. D. & Nance, J. The P4-ATPase TAT-5 inhibits the budding of extracellular vesicles in C. elegans embryos.

Curr. Biol. **21,** 1951–1959 (2011).

16. Jantsch-Plunger, V. & Glotzer, M. Depletion of syntaxins in the early Caenorhabditis elegans embryo reveals a role for membrane fusion events in cytokinesis. *Curr. Biol.* **9,** 738–745 (1999).
17. Benenati, G., Penkov, S., Müller-Reichert, T., Entchev, E. V & Kurzchalia, T. V. Two cytochrome P450s in Caenorhabditis elegans are essential for the organization of eggshell, correct execution of meiosis and the polarization of embryo. *Mech. Dev.* **126,** 382–393 (2009).
18. Florey, O., Kim, S. E., Sandoval, C. P., Haynes, C. M. & Overholtzer, M. Autophagy machinery mediates macroendocytic processing and entotic cell death by targeting single membranes. *Nat. Cell Biol.* **13,** 1335–1343 (2011).
19. Chen, D. *et al.* Clathrin and AP2 Are Required for Phagocytic Receptor-Mediated Apoptotic Cell Clearance in Caenorhabditis elegans. *PLoS Genet.* **9,** 1–18 (2013).
20. Levin, R., Grinstein, S. & Canton, J. The life cycle of phagosomes: formation, maturation, and resolution. *Immunol. Rev.* **273,** 156–179 (2016).
21. Gerace, L. & Tapia, O. Messages from the voices within: regulation of signaling by proteins of the nuclear lamina. *Curr. Opin. Cell Biol.* **52,** 14–21 (2018).
22. Ungricht, R. & Kutay, U. Mechanisms and functions of nuclear envelope remodelling. *Nat. Rev. Mol. Cell Biol.* **18,** 229–245 (2017).
23. González, J. M. & Andrés, V. Synthesis, transport and incorporation into the nuclear envelope of A-type lamins and inner nuclear membrane proteins. *Biochem. Soc. Trans.* **39,** 1758 LP-1763 (2011).
24. Green, R. A. *et al.* The midbody ring scaffolds the abscission machinery in the absence of midbody microtubules. *J. Cell Biol.* **203,** 505–520 (2013).
25. Fazeli, G., Trinkwalder, M., Irmisch, L. & Wehman, A. M. *C. elegans* midbodies are released, phagocytosed and undergo LC3-dependent degradation independent of macroautophagy. *J. Cell Sci.* **129,** 3721–3731 (2016).
26. König, J., Frankel, E. B., Audhya, A. & Müller-Reichert, T. Membrane remodeling during embryonic abscission in *Caenorhabditis elegans*. *J. Cell Biol.* **216,** 1277–1286 (2017).
27. Wang, S. *et al.* A toolkit for GFP-mediated tissue-specific protein degradation in *C. elegans*. *Development* **144,** 2694–2701 (2017).
28. Nishimura, K., Fukagawa, T., Takisawa, H., Kakimoto, T. & Kanemaki, M. An auxin-based degron system for the rapid depletion of proteins in nonplant cells. *Nat. Methods* **6,** 917–922 (2009).
29. Zhang, L., Ward, J. D., Cheng, Z. & Dernburg, A. F. The auxin-inducible degradation (AID) system enables versatile conditional protein depletion in C. elegans.

Development **142,** 4374–4384 (2015).

30. Bobrie, A., Colombo, M., Krumeich, S., Raposo, G. & Théry, C. Diverse subpopulations of vesicles secreted by different intracellular mechanisms are present in exosome preparations obtained by differential ultracentrifugation. *J. Extracell. Vesicles* **1,** (2012).
31. Kowal, J. *et al.* Proteomic comparison defines novel markers to characterize heterogeneous populations of extracellular vesicle subtypes. *Proc. Natl. Acad. Sci.* **113,** E968–E977 (2016).
32. Hell, S. W. Microscopy and its focal switch. *Nat. Methods* **6,** 24–32 (2009).
33. Spiegelhalter, C., Laporte, J. F. & Schwab, Y. Correlative Light and Electron Microscopy: From Live Cell Dynamic to 3D Ultrastructure. in *Electron Microscopy: Methods and Protocols* (ed. Kuo, J.) 485–501 (Humana Press, 2014).
34. Hirayama, S. *et al.* Nuclear export of ubiquitinated proteins via the UBIN-POST system. *Proc. Natl. Acad. Sci. U. S. A.* **115,** E4199–E4208 (2018).
35. Jones, R. D. & Gardner, R. G. Protein quality control in the nucleus. *Curr Opin Cell Biol* **40,** 81–89 (2016).
36. Brenner, S. The genetics of Caenorhabditis elegans. *Genetics* **77,** 71–94 (1974).
37. Praitis, V., Casey, E., Collar, D. & Austin, J. Creation of low-copy integrated transgenic lines in Caenorhabditis elegans. *Genetics* **157,** 1217–1226 (2001).
38. Nance, J. C. elegans PAR-3 and PAR-6 are required for apicobasal asymmetries associated with cell adhesion and gastrulation. *Development* **130,** 5339–5350 (2003).
39. Fraser, A. G. *et al.* Functional genomic analysis of C. elegans chromosome I by systematic RNA interference. *Nature* **408,** 325–330 (2000).
40. Sönnichsen, B. *et al.* Full-genome RNAi profiling of early embryogenesis in Caenorhabditis elegans. *Nature* **434,** 462–469 (2005).
41. Singh, D. & Pohl, C. Coupling of Rotational Cortical Flow, Asymmetric Midbody Positioning, and Spindle Rotation Mediates Dorsoventral Axis Formation in C. elegans. *Dev. Cell* **28,** 253–267 (2014).